II

Publication II

F. Boxberg, T. Häyrynen and J. Tulkki, *Doubling of conductance steps in Si/SiO2 quantum point contact*, Journal of Applied Physics **100**, 024904 (2006).

JOURNAL OF APPLIED PHYSICS **100**, 024904 (2006)

Doubling of conductance steps in Si/SiO_2 quantum point contact

Fredrik Boxberg, Teppo Häyrynen,[a] and Jukka Tulkki
Laboratory of Computational Engineering, Helsinki University of Technology, P.O. Box 9203, FIN-02015 HUT ESPOO, Finland

(Received 25 February 2006; accepted 8 May 2006; published online 19 July 2006)

We have calculated the effect of the oxidation-induced strain on the ballistic conductance in a Si/SiO_2 quantum point contact. The strain-induced deformation potential was calculated semiempirically using a viscoelastic continuum model. The charge carriers are confined to the corners of the waveguide by both the strain-induced deformation potential and the Si/SiO_2 band edge discontinuity. As a consequence nearly degenerate symmetric and antisymmetric transverse states are formed for the Si [001] minima. This additional degeneracy within the Landauer-Büttiker formalism leads to doubling of conductance steps for electrons in the [001] minima which govern the conductance near the cutoff energy. Due to the additional strain-induced confinement, the effective channel width of the quantum point contact is smaller and therefore the conductance steps are sharper. © *2006 American Institute of Physics*. [DOI: 10.1063/1.2214212]

I. INTRODUCTION

Single electron transistors (SET's), quantum wires (QWR's), and quantum point contacts (QPC's) are currently studied intensively to enable their integration with the commercial Si based complementary metal oxide semiconductor (CMOS) technologies. These quantum mechanical transistors offer low power consumption and in the ideal case fluctuation-free operation. The desired quantization of conductance (QC), in QWR's and QPC's, is due to quantum interference (QI). However, this requires a very smooth and well reproducible waveguide potential, which has turned out to be very difficult to obtain using standard CMOS processing techniques.

The original attempts to observe QC in Si failed but led to the discovery of the Coulomb blockade phenomenon in metal oxide semiconductor field-effect transistors (MOSFET's).[1,2] Recently the QC has been studied in QWR's, fabricated using silicon on insulator (SOI) substrates.[3,4] The conductance of these devices, fabricated using conventional Si technologies (electron-beam lithography, etching, and thermal oxidations), exhibited clear Coulomb blockade oscillations[5] characteristic of quantum dots. The reason to this is still not known. The problem might be due to oxide charges, dangling bonds at the Si/SiO_2 interface, and oxidation-related strain effects.[6] These defects could trap electrons and give rise to Coulomb blockade oscillations, if the tunneling times of the trap states were of the right order of magnitude.

In this work we have studied the effect of oxidation-induced strain on the QC in QPC's. The QPC's were fabricated on SOI wafers, using conventional CMOS techniques combined with electron-beam lithography. The used processing technique gives a smooth and well defined Si/SiO_2 interface and a horizontal single-crystal Si channel. However, these structures have still not shown any QC. We have therefore analyzed the possible influence of an oxidation-induced strain on the device characteristics. We have used a semiempirical oxidation model based on detailed transmission electron micrographs (TEM's) of the fabricated waveguide structures.[7] Our oxidation model was developed from hydrodynamic oxidation models[8,9] for the calculation of the post-oxidation strain field.

II. OXIDATION-INDUCED STRAIN

The first thin oxide layer, on a Si surface, is formed through an initial surface oxidation process. Thereafter, the thermal oxidation enters a continuous oxygen diffusion-reaction stage where the O atoms diffuse through SiO_2 and react with Si at the Si/SiO_2 interface. The oxygen concentration and the volume of the SiO_2 can be considered constant during the oxidation. However, since there is a steady diffusion of O atoms to the Si/SiO_2 interface, there is an internal volume growth (material is added into the structure) that strains the structure. It has been shown that the strain depends on the curvature of the interface and that furthermore, the O diffusion and the reaction constant depend on the strain.[8,10] Depending on the oxidation process and the temperature ramp down after the oxidation, the oxidation-induced strain might persist and also influence the electronic properties of the final Si/SiO_2 device.[11] It is, however, very difficult to observe or measure the internal strain directly and one has to rely on semiempirical models.

Conventionally the thermal oxidation is modeled by iterative schemes (see, e.g., Refs. 12–14). The local strain, diffusion, and reaction rates are updated for each time step. This technique is, however, computationally infeasible for large device geometries. We have, therefore, developed a simplified and phenomenological three dimensional (3D) oxidation model. The Si/SiO_2 geometry is taken from TEM cross sections of fabricated SOI waveguides,[7,15] and the strain is computed by elastic expansion of only one thin phenomenological interface layer at the Si/SiO_2 interface.[16] The expansion of the oxygen interface layer is anisotropic and always perpendicular to the Si/SiO_2 interface. This induces a

[a]Electronic mail: tihayryn@lce.hut.fi

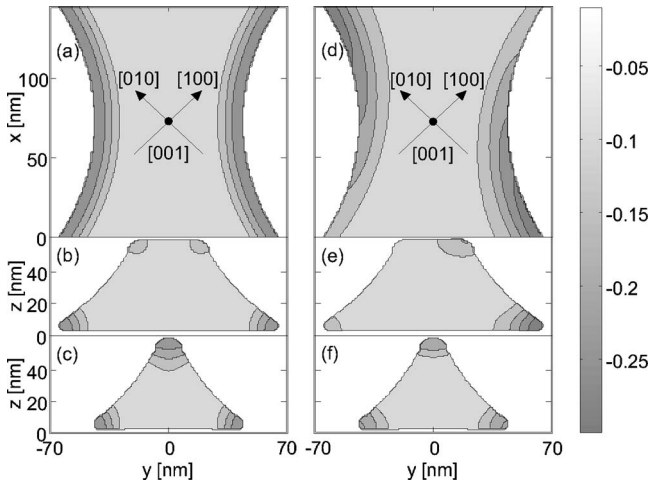

FIG. 1. Strain-induced potential profile of the QPC. (a) Potential of electrons in [001] minima 7 nm above the bottom. (b) Cross-sectional potential at the end of the QPC. (c) Cross-sectional potential in the middle of the QPC. [(d)–(f)] Corresponding potential profiles of electrons in [010] minima.

strain, which is proportional to the curvature of the interface in accordance with the hydrodynamical models.[8,9] The single crystal Si and the amorphous SiO_2 were modeled as cubic lattice and isotropic materials, respectively. By appropriate choice of the interface thickness and the volume expansion, our model reproduces the strain field of analytical hydrodynamical models of thermal oxidation in cylindrical geometries.[8,10] We also expect that the predictivity of our model is fair for the actual fabricated QPC's.[7]

The interface expansion and the strain were computed using the continuum elasticity theory and the finite element method (FEM). The elastic constants and deformation potentials are given in Ref. 16. The calculated strain field contained sharp minima along the corners of the Si channel, where the local curvature radius was even less than 10 nm. The strain field had, therefore, to be smoothened for the ballistic conductance calculations, because the conductance of Si/SiO_2 QPC is very sensitive to the numerical accuracy of the FEM calculation. For this, we used a moving average filter, where the potential in the Si was convoluted several times over a $6\times6\times6$ nm^3 sampling volume. The smoothened potential is shown in Fig. 1.

III. BALLISTIC CONDUCTANCE

A. Scattering parameters

We used the Landauer-Büttiker formalism[17] to calculate the conductance. In this formalism a scatterer (nonideal waveguide) is connected to two electron reservoirs via ideal leads. Let μ_S and μ_D represent the chemical potentials at source and drain reservoirs, respectively, and let $V_b=(\mu_S-\mu_D)/e$ be a small bias voltage. The conductance formula is then given by[17]

$$G(\mu_S)=\frac{2e^2}{h}\int T(\varepsilon)\left[-\frac{\partial f(\mu_S,\varepsilon)}{\partial\varepsilon}\right]d\varepsilon, \tag{1}$$

where $T(\varepsilon)$ is the total transmission trough the scatterer at energy ε and $f(\mu_S,\varepsilon)=\{1+\exp[(\varepsilon-\mu_S)/(k_BT)]\}^{-1}$ is the Fermi-Dirac distribution of the source reservoir. We furthermore used the mode-matching method[18] to calculate the scattering matrix $\mathbf{S}_{SD}$ from source to drain. The total transmission through the QPC is given by

$$T=\sum_n \frac{\sum_m S_{SD}(m,n)S_{SD}^*(m,n)[k_D(m)+k_D^*(m)]}{k_S(n)+k_S^*(n)}, \tag{2}$$

where the subscripts S and D correspond to source and drain, respectively, n goes trough all active channels (or transverse modes) in the source, and m represents the channels in the drain. Furthermore the wave vectors $k_S(j)$ and $k_D(j)$ are given by $k_{S,D}(j)=\sqrt{2m_x^*[\varepsilon-\varepsilon_{S,D}(j)]\hbar^{-2}}$, where ε is the total energy and $\varepsilon_{S,D}(j)$ is the cutoff energy of mode j.

B. Transverse eigenstates

The conduction band of silicon has six minima along the equivalent $\langle100\rangle$ axes. The effective mass along the respective $\langle100\rangle$ axis is the longitudinal effective mass $m_l^*=0.98m_0$, and the effective mass perpendicular to the axis is the transverse effective mass $m_t^*=0.19m_0$.

The QPC is on the (001) plane in the $\langle110\rangle$ direction. We have used a coordinate system where the x coordinate is along the QPC and y and z are the horizontal and vertical coordinates of the cross section of the QPC (see Fig. 1). We have three separate cases for the effective masses in the rotated coordinates[19] ($\theta=\pi/4$): For the [100] minima the masses are $m_x^*=[(\sin^2\theta)/m_t^*+(\cos^2\theta)/m_l^*]^{-1}=0.318m_0$, $m_y^*=m_l^*\sin^2\theta+m_t^*\cos^2\theta=0.585m_0$, and $m_z^*=m_t^*=0.19m_0$. For the [010] minima the masses are $m_x^*=[(\cos^2\theta)/m_t^*+(\sin^2\theta)/m_l^*]^{-1}=0.318m_0$, $m_y^*=m_l^*\cos^2\theta+m_t^*\sin^2\theta=0.585m_0$, and $m_z^*=m_t^*=0.19m_0$. For the [001] minima the masses are $m_x^*=m_y^*=m_t^*=0.19m_0$ and $m_z^*=m_l^*=0.98m_0$. Thus we must solve the effective mass Schrödinger equation separately for the [100], [010], and [001] minima ([100] and [010] minima are equivalent if $\theta=\pi/4$). Furthermore the unit of conductance becomes $2(2e^2/h)$ due to the two equivalent conduction band minima for each $\langle100\rangle$ axis. We solved the transverse modes of the smoothened QPC potential at 1 nm intervals using finite difference, and we used the mode-matching method to obtain the scattering matrix. Then the transmission coefficients and the conductance were obtained using Eqs. (2) and (1).

C. Results and discussion

Figure 2(a) shows the conductance of the nonstrained QPC at the temperatures of 1 and 4 K. We can distinguish conductance steps at 1 K, but the steps are almost vanished at 4 K because the transverse energies are so close that the integral (1) includes several eigenstates already at the very low temperatures.

Figures 2(b) and 2(c) show the conductance of the same QPC with the strain-induced potential at the temperatures of 4 and 20 K. Figure 2(b) shows the conductance for electrons in [001] minima and Fig. 2(c) for electrons in [100]/[010] minima. The conductances of [100] and [010] minima are

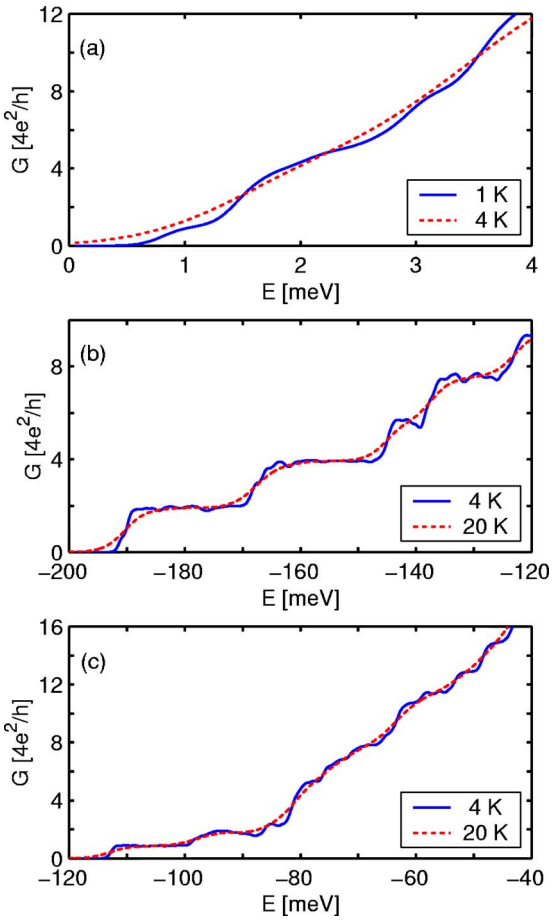

FIG. 2. (Color online) (a) The total conductance of the nonstrained QPC as a function of the Fermi energy measured from the Si conduction band edge. (b) Conductance of the [001] minima when the strain-induced potential is included in the calculations of transverse eigenstates. (c) Conductance of the [100]/[010] minima when the strain-induced potential is included in the calculations of transverse eigenstates.

equal, because for [100] and [010] minima the strain-induced potential is inversion symmetric in the plane of the QPC

Due to the strain-induced potential the transverse eigenstates become localized to the corners of the QPC. Thus the spacing of eigenenergies is much larger, and accordingly the conductance differs dramatically from that of the nonstrained QPC. By examining the potential profiles in Fig. 1, one can observe that the potential for [001] electrons is symmetric in each transverse slice. Furthermore the potential for [100]/[010] electrons is symmetric only in the middle of the QPC [see Fig. 1(f)], and at the ends of the QPC the potential minima are located only on one side of the transverse slice [see Fig. 1(d)].

Figures 2(a)–2(c) show two large differences in the conductance of non-strained and strained QPC's: The conductance steps are sharpened by the strain, and the height of the first conductance steps is doubled (becoming $8e^2/h$). At larger Fermi energies the conductance of the strained QPC approaches that of the nonstrained structure.

Figure 3 shows the eigenfunctions of the two lowest transverse states of the [001] minima. These transverse modes dominate the conductance at threshold. The lowest eigenstates for the [001] minima are localized symmetrically

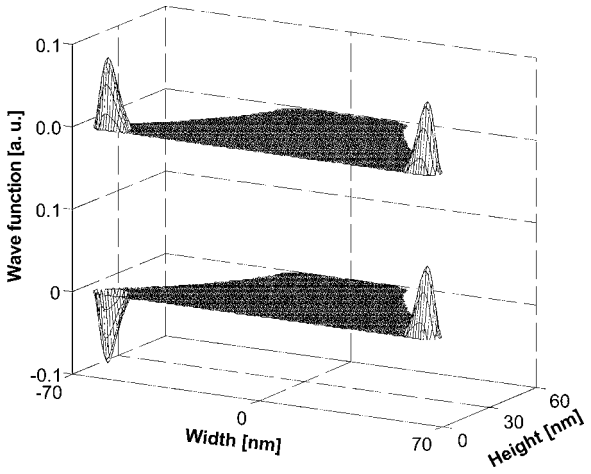

FIG. 3. The first two transverse eigenstates at the end of the strained QPC. The states are nearly degenerate. Above is the symmetric state and below is the antisymmetric state.

to the corners of the QPC (cf. Fig. 1). The strain-induced potential gives rise to a weak coupling of electronic orbitals localized in the potential minima at the lower corners of the QPC (see Fig. 3). The resulting symmetric and antisymmetric states are nearly degenerate, and therefore the size of conductance step is 2 $[2(2e^2/h)]$ (see Fig. 2). At higher energies the transverse states also localize to the upper corners of the QPC.

The first conducting transverse modes of the [100] and [010] minima are located diagonally in the upper corners of the QPC [see Figs. 1(d)–1(f)]. The conducting channel goes diagonally through the QPC because the upper corner potential energy minima merge in the middle of the QPC. Thus there is only one conducting channel (in both [100] and [010] minima), and the conductance step size is 1 $[2(2e^2/h)]$ near the threshold of these minima.

The present calculation is based on a phenomenological model of the thermal oxidation process. The most critical approximations involved are the use of only one oxidation-induced volume expansion in the geometry and the rough estimation of the absolute level of the post-oxidation strain. In spite of these approximations, the model leads to a very heavy computational problem. Although we used in the current model $\sim 10^5$ elements, the numerical accuracy had to be improved by a thorough smoothening procedure of the simulated strain data. With further computational efforts the oxidation model could be formulated within the mean-field-like theory[12–14] to account for the time dependence of true oxidation process. Even within the mean field theory, all calculations rely upon poorly known process parameters and constants, such as a stress-dependent viscosity and anisotropic reaction rates. This greatly limits the accuracy of such a simulation and its physical justifications.

IV. CONCLUSIONS

In conclusion, we have shown that the strain-induced potential localizes the transverse modes to the corners of the Si/SiO_2 QPC. The degenerate symmetric and antisymmetric transverse states produce two symmetrically located con-

ducting channels inside the QPC which leads to conductance step size of $8e^2/h$ near the cutoff energy. The conductance steps become also much more prominent than in the corresponding nonstrained QPC, and they are also resolved at much higher temperatures due to the larger energy spacing of transverse states.

The conductance quantization has been reported previously in several silicon QWR structures,[3,20] but there are very few conductance measurements of silicon QPC's (Ref. 21) that have shown well resolved conductance steps. It is difficult to compare our calculations with the measurements reported in Ref. 21 because this QPC structure is not processed using the same oxidation-induced confinement method. Therefore the role of strain (if any) would be presumably different in this case. The QPC structure exhibits, however, conductance steps at selected gate voltages. In this structure the quantization step of $8e^2/h$ is obviously due to [100] and [010] valley degeneracies. In the oxidized Si channels the conductance is dominated by Coulomb-blockade-like features. Accordingly, conductance quantization predicted in our work is not visible in the QPC fabricated so far.

[1] J. H. F. Scott-Thomas, S. B. Field, M. A. Kastner, H. I. Smith, and D. A. Antoniads, Phys. Rev. Lett. **62**, 583 (1989).
[2] H. Ishikuro and T. Hiramoto, Appl. Phys. Lett. **71**, 3691 (1997).
[3] Y. Nakajima, Y. Takahashi, S. Horiguchi, K. Iwadate, H. Namatsu, K. Kurihara, and M. Tabe, Appl. Phys. Lett. **65**, 2833 (1994).
[4] Y. Takahashi, A. Fujiwara, and K. Murase, Semicond. Sci. Technol. **13**, 1047 (1998).
[5] A. T. Tilke, F. C. Simmel, H. Lorenz, R. H. Blick, and J. P. Kotthaus, Phys. Rev. B **68**, 075311 (2003).
[6] Y. Shi, H. Ishikuro, and T. Hiramoto, J. Appl. Phys. **84**, 2358 (1998).
[7] J. Ahopelto *et al.*, Silicon Nanoelectronics Workshop, Workshop Abstracts 2000 (unpublished), 79–80.
[8] D. Kao, J. P. McVittie, W. D. Nix, and K. C. Saraswat, IEEE Trans. Electron Devices **35**, 25 (1988).
[9] V. Senez, D. Collard, P. Ferreira, and B. Baccus, IEEE Trans. Electron Devices **43**, 720 (1996).
[10] D. Kao, J. P. McVittie, W. D. Nix, and K. C. Saraswat, IEEE Trans. Electron Devices **34**, 1008 (1987).
[11] H. Namatsu, S. Horiguchi, M. Nagase, and K. Kurihara, J. Vac. Sci. Technol. B **15**, 1688 (1997).
[12] V. S. Rao and T. J. R. Hughes, Int. J. Numer. Methods Eng. **47**, 341 (2000).
[13] V. S. Rao, T. J. R. Hughes, and K. Garikipati, Int. J. Numer. Methods Eng. **47**, 359 (2000).
[14] P. Causin, M. Restelli, and R. Sacco, Comput. Methods Appl. Mech. Eng. **193**, 3687 (2004).
[15] A. Gustafsson, J. Ahopelto, M. Kamp, M. Emmerling, and A. Forchel, Inst. Phys. Conf. Ser. **164**, 455 (1999).
[16] F. Boxberg and J. Tulkki, IEEE Trans. Electron Devices **48**, 2405 (2001).
[17] S. Datta, *Electronic Transport in Mesoscopic Systems* (Cambridge University Press, Cambridge, 1995).
[18] A. Weisshaar, J. Lary, S. M. Goodnick, and V. K. Tripathi, J. Appl. Phys. **70**, 355 (1991).
[19] S. Horiguchi, Y. Nakajima, Y. Takahashi, and M. Tabe, Jpn. J. Appl. Phys., Part 1 **34**, 5489 (1995).
[20] K. Hishiguchi and S. Oda, J. Appl. Phys. **92**, 1399 (2002).
[21] A. Ohata and A. Toriumi, Jpn. J. Appl. Phys., Part 1 **42**, 1552 (2003).